Online Optimizer for Distribution Networks on Neplan

Original Citation:
F. Cappelluti, A. Khalili, M. Gioannini, "Open Circuit Voltage Recovery in Quantum Dot Solar Cells: a Numerical Study on the Impact of Wetting Layer and Doping," *IET Optoelectronics* (2016).
DOI: 10.1049/iet-opt.2016.0069

Open Circuit Voltage Recovery in Quantum Dot Solar Cells: a Numerical Study on the Impact of Wetting Layer and Doping

Federica Cappelluti, Arastoo Khalili, Mariangela Gioannini
Department of Electronics and Telecommunications, Politecnico di Torino, Corso Duca degli Abruzzi 24, 10129 Torino, Italy
E-mail: federica.cappelluti@polito.it

ABSTRACT

We present a numerical study on the influence of wetting layer states and doping on the photovoltage loss of InAs/GaAs quantum dot solar cells. Quantum-mechanical simulations are used to analyze how the reduction of wetting layer by Al(Ga)As overgrowth changes the quantum dot electronic states. Device-level simulations allows to correlate such changes with the achievable open circuit voltage. Almost full open circuit voltage recovery is predicted by combining wetting layer reduction, to realize thermal decoupling of barrier and quantum dot confined states, and doping to suppress radiative recombination through the quantum dot confined states.

I. INTRODUCTION

Photovoltage degradation in InAs/GaAs Quantum Dot (QD) solar cells largely undermines the expected efficiency gain with respect to single-junction solar cells [1,2]. Among the most fundamental issues are the strong capture and recombination of photogenerated carriers through the QD confined states, thermally coupled to the barrier states through the extended wetting layer (WL) states [3,4]. Selective doping of QDs, through direct-doping or modulation-doping techniques, has been proposed and demonstrated as useful means to mitigate the open circuit voltage degradation [5]–[8]. Since reported devices are typically plagued by significant non radiative recombination caused by the defects formed during the QD growth, there is a quite general consensus on the effectiveness of doping in passivating such defects, while its effectiveness in suppressing QD radiative recombination remains somewhat controversial. In [8] remarkable $V_{\rm oc}$ recovery was observed despite an evident increase of non radiative recombination, making the authors to argue that substantial thermal decoupling of QD and barrier states, and thus suppression of QD radiative recombination, was attained. Numerical simulations [9] accounting for trapping and recombination mechanisms through QDs and their competition with barrier recombination have demonstrated that even in the radiative limit, assuming non defective crystal, remarkable $V_{\rm oc}$ recovery might be attained by doping owing to the strong suppression of QD radiative recombination. In this case the radiative recombination through WL states remains as the limiting factor of the achievable $V_{\rm oc}$. As an alternative or complementary means to QD doping, WL reduction by capping the QDs with AlAs layers [10]–[13] has also been proposed to achieve thermal decoupling between QD confined states and barrier and prevent the capture of photogenerated carriers. In [13], through the combined use of doping, AlAs capping of QDs and overgrowth with AlGaAs, full $V_{\rm oc}$ recovery was demonstrated and correlated through structural characterizations to the effective reduction of the wetting layer.

In this work we investigate the impact of wetting layer states and doping on the open circuit voltage of QDSCs through device-level simulations complemented by quantum-mechanical calculations to correlate the QD morphology and electronic structure. Based on the numerical results, we introduce a simple analytical model that highlights the competition between barrier and QD recombination mechanisms and correlates the effective QD capture rate to the achievable open circuit voltage.

II. MODEL

To study the effect of the presence of the InAs wetting layer and of possible additional AlGaAs layers on the QD energy states we used the nextnano software [14]. The strain distribution is determined using continuum elastic theory and minimizing the free energy within the crystal, and energy bands are calculated taking into account the potential induced by the strain deformation. QD energy levels are calculated by solving the 3D Schrödinger equation with the 8-band $k \cdot p$ method.

Then, we correlate the QD electronic structure and solar cell performance through device-level simulations using the *QD-aware* modelling approach described in [3]. The model exploits a drift-diffusion-Poisson formulation coupled with a set of rate equations (RE) describing the QD carrier dynamics. At each QD layer, the barrier continuity equation for electrons (and similarly for holes) reads as

$$\frac{\partial n}{\partial t} = \frac{1}{q}\frac{\partial J_n}{\partial x} - U_n^{\rm B} + G_{ph}^{\rm B} - \left(R_{n,\rm CAP}^{\rm B\to WL} - R_{n,\rm ESC}^{\rm WL\to B}\right) \qquad (1)$$

where $U_{n,\rm B}$ is the barrier net recombination rate, $G_{ph,\rm B}$ is the barrier photogeneration rate, and the net electron capture rate $(R_{n,\rm CAP}^{\rm B\to WL} - R_{n,\rm ESC}^{\rm WL\to B})$ describes the local, WL-mediated interaction of barrier and QD states. Subband charge transfer within QD states is then modeled by a three-level RE system, involving WL, excited state (ES), and ground state (GS), and

accounting for band-to-band recombination and photogeneration through QD states. The complete model formulation is reported in [3]. For the sake of the following discussion, we may notice that depending on the solar cell operating point eq. (1) highlights the role of QDs as photogeneration centers when the escape from the WL dominates with respect to the capture rate (e.g. at short circuit) or as recombination centers when the capture dominates with repect to the escape (e.g at open circuit, through catpure in the WL and subsequent relaxation in the QD confined states). In the following simulations, we assume pure thermal escape of carriers, neglecting escape via field-assisted tunneling and two-photon absorption.

III. Results and Discussion

A. QD electronic structure

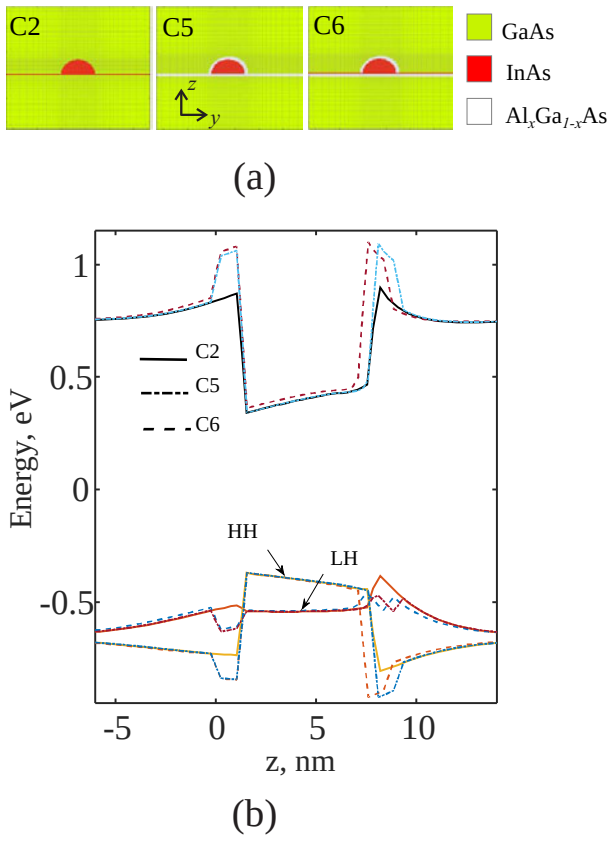

Fig. 1. (a) Cross-section of the studied QD configurations. (b) Energy band structure along the growth direction (z-axis), at QD base center, for the various structures in (a) calculated accounting for the strain distribution.

As case study we consider conventional InAs/GaAs QDs and QDs embedded in AlGaAs layers. The QDs are modelled as lens-shaped InAs QDs with circular base with radius 14 nm and height of 6 nm. We analyze three different configurations whose cross-section is sketched in Fig. 1(a):

- InAs QD with 0.5 nm thick WL (sample C2)
- InAs QD grown over a 1.3 nm thick layer $Al_xGa_{1-x}As$ and capped with a 1.3 nm layer of $Al_xGa_{1-x}As$ (sample C5)
- InAs QD with 0.5 nm thick InAs WL grown over a 1.3 nm thick $Al_xGa_{1-x}As$ layer and capped with a 1.3 nm layer of $Al_xGa_{1-x}As$ (sample C6).

The molar fraction of $Al_xGa_{1-x}As$ ranges from $x = 0.05$ to $x = 0.2$. Samples C5 and C6 differ for the presence of the InAs WL; their comparative analysis allows to assess the effect on the QD electronic states of the physical reduction of the InAs wetting layer during the QD growth. We assume that the QD layers will be separated by 25 nm of GaAs layer. Thus, strain relaxation is calculated within a GaAs volume of about 50 nm x 50 nm x 50 nm, imposing periodic boundary conditions at the box edges. According to the GaAs zincblende structure, x-axis, y-axis, z-axes are associated to the crystal orientation axes [100], [010],[001], respectively, with z corresponding to the QD growth direction.

The calculated energy band structure is reported in Fig. 1(b). Strain relaxation along the thin (0.5 nm) wetting layer results negligible, as already reported in previous works [15]. Therefore the QD configurations with and without wetting layer have similar energy bands, with almost identical height of the potential wells, and the primary effect of the wetting layer is to increase the effective height of the QD. This turns into deeper confined states for samples with the wetting layer (C2 and C6) with respect to the sample without it. In order to assess the effect on the QD energy levels of the insertion of $Al_xGa_{1-x}As$ barriers, we performed preliminary simulations using the single-band effective mass approximation. Fig. 2 shows the calculated shift of the GS transition energy of the configurations with the barriers with respect to the InAs/GaAs QD (C2). Sample C5 - with $Al_xGa_{1-x}As$ layers but without InAs wetting layer - presents an energy shift of the GS state about four times larger than sample C6 - with $Al_xGa_{1-x}As$ layers and InAs wetting layer. In fact, the QD structure with deeper confinement is less sensitive to the increase of the potential height induced by the $Al_xGa_{1-x}As$ layers. The analysis was then refined for sample C2 and C5 by using the 8-band $k \cdot p$ method, to study the behavior of the higher energy states. The calculated shift of the transition energy for the WL states of the C5 sample - with respect to the C2 one - are approximately 60 meV and 80 meV for Al fraction of 0.05 and 0.2, respectively. In the same range of Al molar fraction, the GS state shift amounts to 40 meV and 50 meV. Of the same sign are the results in [11], where photoresponse measurements showed a significant WL blue shift - of about 30 meV - for QDs surrounded by $Al_{0.05}Ga_{0.95}As$ barriers with respect to conventional InAs/GaAs QDs, that was explained in view of a reduction of the QD size and in particular of the wetting layer, as later confirmed by the structural characterizations of similar samples in [13].

B. Effect of WL States on Photovoltage

Correlation between QD media and solar cell performance is studied considering a simple GaAs-only solar cell (i.e. without widegap window and back surface field layers), whose intrinsic region is made by a stack of 20 QD layers separated by GaAs spacer layers of about 50 nm thickness. The detailed description of the cell structure is summarized in Table I. In [9] we studied the same cell to assess the effect of selective doping on photovoltaic behavior and photoluminescence. The QD media assumed in [9] is taken as reference: these QDs

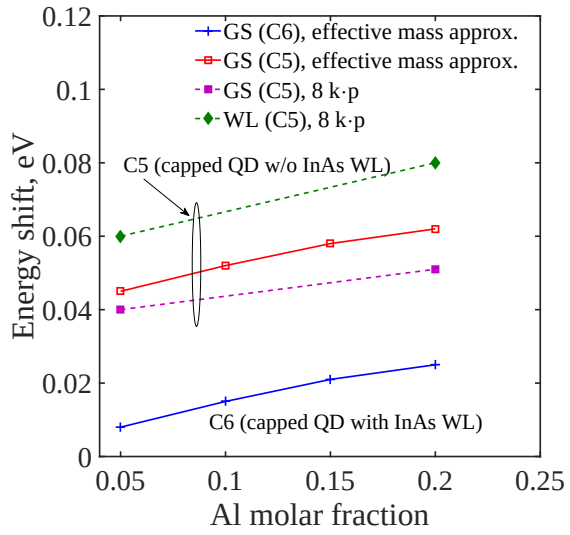

Fig. 2. Change of the WL and GS transition energy with respect to the C2 reference as a function of Al molar fraction for the various configurations including $Al_xGa_{1-x}As$ barriers.

TABLE I
CELL STRUCTURE AND REFERENCE QD PARAMETERS

Cell structure	
Layer	Thickness [nm]
p^+ (5×10^{18} cm^{-3}) GaAs	50
p (1×10^{18} cm^{-3}) GaAs	100
QD region, intrinsic GaAs	1000
intrinsic GaAs	50
n^+ (1×10^{18} cm^{-3}) GaAs	300
QD parameters	
QD density, N_{QD}, [cm^{-2}]	6×10^{10}
State degeneracy, $g_{ES}^{e,h}$, $g_{GS}^{e,h}$	4, 2
WL Density of States, $N_{WL}^{e,h}$, [cm^{-2}]	2.4×10^{12}
$\Delta E_{B\text{-}WL}^{e}$, $\Delta E_{WL\text{-}ES}^{e}$, $\Delta E_{ES\text{-}GS}^{e}$, [meV]	140, 62, 70
$\Delta E_{B\text{-}WL}^{h}$, $\Delta E_{WL\text{-}ES}^{h}$, $\Delta E_{ES\text{-}GS}^{h}$, [meV]	4, 4, 16
$\tau_{CAP,\,B\to WL}^{e}$, $\tau_{CAP,\,WL\to ES}^{e}$, $\tau_{CAP,\,ES\to GS}^{e}$, [ps]	0.3, 1.2, 1.2
$\tau_{CAP,\,B\to WL}^{h}$, $\tau_{CAP,\,WL\to ES}^{h}$, $\tau_{CAP,\,ES\to GS}^{h}$, [ps]	0.1, 0.1, 0.1
τ_r^{WL}, τ_r^{ES}, τ_r^{GS}, [ns]	1, 1, 1
Peak optical absorption, α_{WL}, α_{ES}, α_{GS}, [cm^{-1}]	10^4, 900, 400
QD thickness, t_{QD}, [nm]	4

are characterized by WL, ES, and GS energy states at about 1.29, 1.22 and 1.13 eV with inter-level spacings and capture and relaxation time constants specified in Table I. Based on the simulations in Sec. III-A, the influence of $Al_xGa_{1-x}As$ barriers embedding the QDs is studied in terms of shift of the WL energy state in the conduction band with respect to the reference QD media. We focus on electron states only, since hole states are found to be shallower and with a small energy separation, providing a very efficient thermal coupling to the barrier, for all the studied QD configurations. For the sake of simplicity we neglect the simultaneous GS and ES levels shift: at high doping levels the photovoltage is not influenced by these levels and therefore the hypothesis does not affect the amount of photovoltage recovery; on the other hand, for the undoped or low doping case, the hypothesis provides a worst-case prediction of achievable V_{oc}. In [9] we have shown that comparable voltage recovery may be expected regardless of the specific doping technique for QDs. In the following we restrict the analysis to directly-doped cells, where direct-doping is modelled by placing a 5 nm thick δ-doping layer at each QD layer. The sheet density of dopants is set to a multiple (α) of the QD density so as to nominally provide α carriers per dot. Simulations, carried out at ambient temperature ($T = 300$ K) include barrier radiative recombination, with radiative coefficient set to 2.0×10^{-10} cm^{3}s^{-1}, and defect induced non-radiative recombination with Shockley Read Hall (SRH) carrier lifetime of 500 ns, corresponding to a high quality barrier, working close to the radiative limit. Radiative lifetime in QD states is set to 1 ns.

Fig. 3 shows the External Quantum Efficiency (EQE) of undoped cells with QD media with WL confinement energy ($\Delta E_{B\text{-}WL}^{e}$) reduced from 140 meV (reference QD) to 60 meV. Besides WL shift and consequent reduction of the harvested light spectral range, a slight decrease of ES and GS states is observed due to the decreased thermal coupling between these

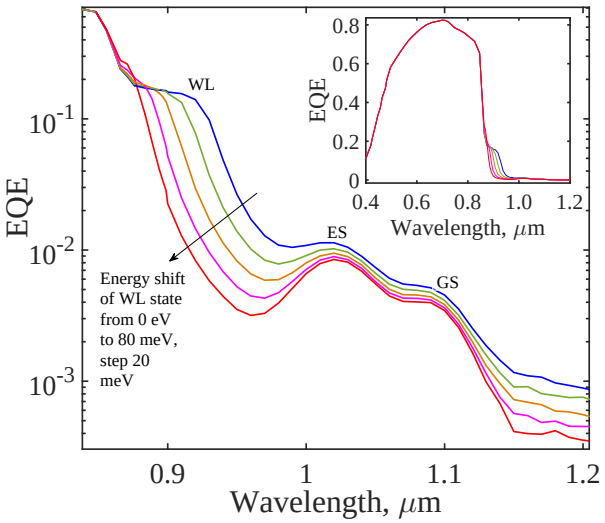

Fig. 3. Calculated external quantum efficiency for WL confinement, $\Delta E_{B\text{-}WL}^{e}$, ranging between 140 meV and 60 meV. The inset shows the EQE in the whole spectral range.

states and the WL one. The penalty is however negligible in terms of total QD photogeneration and will be even smaller if concomitant upward shift of GS and ES is accounted for.

Fig. 4 analyses the combined effect of WL shift and selective doping on the achievable open circuit voltage. For the sake of reference, a baseline GaAs cell with the same geometry reaches a V_{oc} of 0.953 eV. The undoped cell is insensitive to the WL position, since the photovoltage loss is dominated by the radiative recombination across the confined ES and GS states. As doping is introduced, carrier capture in these states is reduced by strengthening the thermal escape from

the QDs (i.e. moving the WL state closer to the barrier) and remarkable loss mitigation is possible, by blocking via doping the further relaxation in the GS and ES, that would otherwise behave as very efficient recombination centers. For the larger WL confinement, selective doping allows for a V_{oc} recovery of about 80 mV, that increases to about 110 mV for the reduced WL cell, attaining almost full V_{oc} recovery ($V_{oc} = 0.950$). The results compare very well with literature data of similar structures, where maximum demonstrated V_{oc} recovery ranges between 120 mV in the modulation-doped cells in [7] to 105 mV in the direct-doped cells in [8].

The raise of photovoltage with doping density becomes larger as WL state is less confined owing to the reduced thermal coupling via WL states between barrier and QD confined states. As shown in Fig. 5, this leads to a more efficient filling of ES and GS states through doping. Thus, reduction of the WL somewhat relaxes the amount of doping level required for attaining large V_{oc} recovery. As a matter of fact, high density doping could even deteriorate the material quality inducing further nonradiative recombination centers [6,12]. Moreover, doping obviously causes some penalty in the achievable QD photogeneration. Thus, engineering QD shape and size combined with doping could provide a better trade-off in terms of power conversion efficiency. In the present case study, the cell with deeper WL reaches a maximum efficiency of 16.6% at 15e/dot, while the cell with shallower WL reaches an optimum efficiency of 17.24% (slightly lower than the reference cell optimum efficiency of 17.28%) at 10 e/dot doping level. These results are very encouraging, considering that the model completely neglects any mechanism that could mitigate thermalization losses, such as two-photon absorption [16] or carrier escape through scattering with hot electrons [17,18]. Furthermore, even in such situation, enhancing QD photogeneration, e.g. through light-trapping approaches, could make the QD cell to overcome its bulk counterpart [19].

Once capture and recombination through GS and ES have been suppressed, WL states remain as the ultimate recombination channel loss induced by QDs. The reduction of WL confinement and the enhanced thermal coupling between WL and barrier weakens the effective capture rate in WL, as evidenced by the decrease of WL states occupation probability as WL energy shifts towards the barrier. This turns into a decreased room temperature photoluminescence in capped QDs as experimentally observed in [13], and yields the full recovery of V_{oc} observed in Fig. 4.

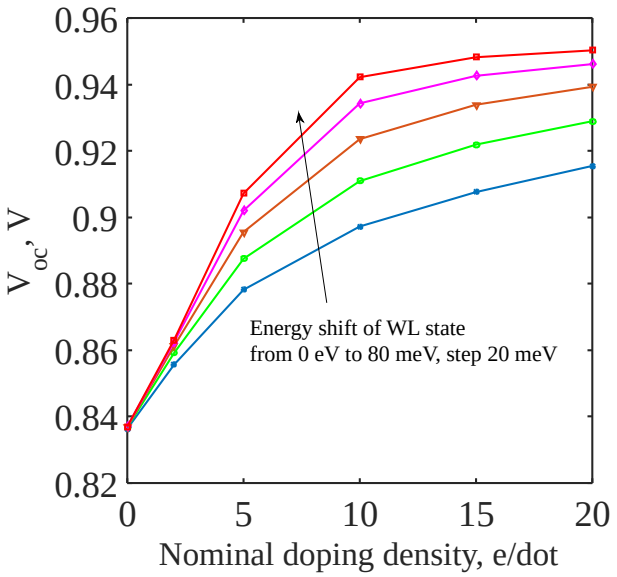

Fig. 4. Open circuit voltage as a function of the nominal per dot density and WL confinement. Simulations were done under 1 sun AM1.5 G illumination.

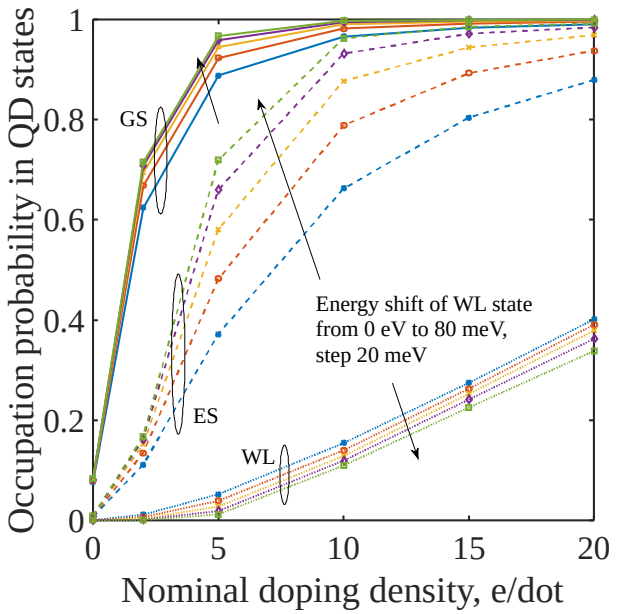

Fig. 5. Occupation probability in the QD states - at open circuit condition - as a function of the nominal per dot density and WL confinement.

C. Correlation between V_{oc} penalty and effective QD capture time

The competition between barrier and QD recombination channels and their influence on the cell photovoltage may be clearly appraised by analyzing the free charge balance across the cell at open circuit. Under DC condition, by using first-order lifetime approximations for the net barrier recombination terms and the net QD capture rate, eq. 1 can be recast as

$$\frac{1}{q}\frac{\partial J_n}{\partial x} - \frac{n}{\tau_{\text{eff}}^{\text{B}}} - \frac{n}{\tau_{\text{eff}}^{\text{QD}}} + G_{ph}^{\text{B}} = 0 \qquad (2)$$

where the lifetimes $\tau_{\text{eff}}^{\text{B}}$, τ_{eff}^{QD} represent the equivalent effective lifetime for recombination mechanisms involving barrier states [20] and the effective QD capture (and subsequent recombination) time through QD states, respectively. At open circuit the cell operates close to flat-band condition, thus $\partial J_n/\partial x = 0$. Using the junction law ($n \approx n_0 \exp(V/V_T)$, n_0 being the thermal equilibrium electron density), eq. 2 yields an approximate compact expression for the open circuit voltage, from which we can estimate the penalty, ΔV_{oc}, induced by the QDs:

$$\Delta V_{oc} \approx V_T \ln\left(1 + \frac{\tau_{\text{eff}}^{\text{B}}}{\tau_{\text{eff}}^{\text{QD}}}\right). \qquad (3)$$

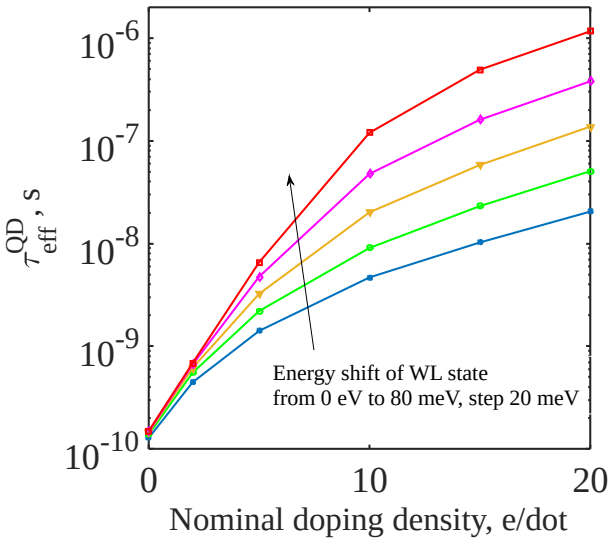

Fig. 6. Effective QD capture time estimated from the numerical simulations at open circuit condition.

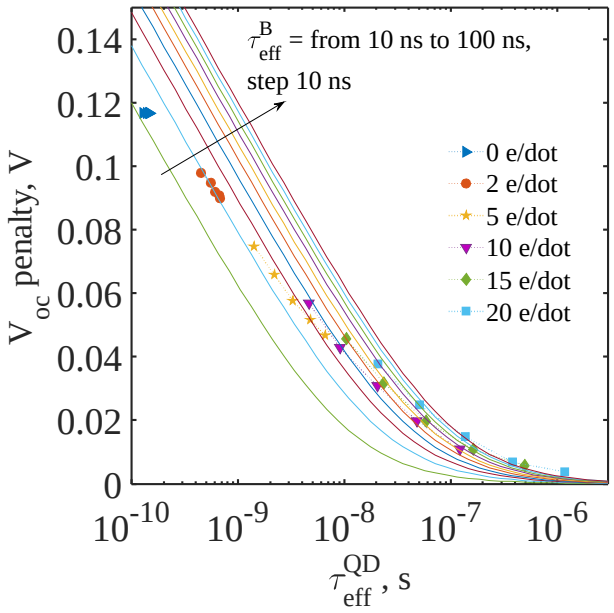

Fig. 7. Correlation between the V_{oc} penalty and effective QD capture time in Fig.6. Symbols are the results of numerical simulations, grouped by doping level and for WL confinement changing from 140 to 60 meV. Solid lines represent the V_{oc} penalty calculated according to eq.3.

Clearly, when $\tau_{\text{eff}}^{QD} \ll \tau_{\text{eff}}^{\text{B}}$, e.g. in the undoped cell, $\Delta V_{oc} \approx V_T \ln\left(\tau_{\text{eff}}^{\text{B}}/\tau_{\text{eff}}^{\text{QD}}\right)$, when $\tau_{\text{eff}}^{\text{QD}} \gg \tau_{\text{eff}}^{\text{B}}$, $\Delta V_{oc} \approx 0$. The effective QD capture time, estimated as the ratio between the average carrier density and the average net capture rate across the QD region, is analyzed in Fig. 6 as a function of doping density and barrier-WL energy spacing. At low doping levels, τ_{eff}^{QD} is weakly dependent on WL state confinement and increases exponentially with the doping density in agreement with the theoretical predictions in [21] and experimental data in [22]. Namely, considering the thermally activated nature of the process, we find that τ_{eff}^{QD} grows as $\exp\left[K_\alpha \alpha / k_{\text{B}} T\right]$, with $K_\alpha = 15 - 20$ meV/(e/dot) depending on the doping density. At larger doping levels, the increase of τ_{eff}^{QD} with doping is slower, due to the large density of states available in the WL. However, the reduced WL confinement causes a marked reduction of carriers capture in QDs, owing to the decreased WL occupation probability seen in Fig. 5.

Finally, Fig. 7 maps the open circuit voltage penalty of QD cells, ΔV_{oc}, as a function of the effective QD capture time for the different doping levels and WL energies. Numerical data show a good correlation with the analytical expression in eq. 3. The deviation from a pure exponential dependence can be understood taking into account that doping influences, besides QD dynamics, the potential profile and non radiative recombination in the barrier [9]. For increasing doping levels, the equivalent barrier lifetime in eq. 3 must be increased from 10 ns to 100 ns to follow the trend shown by the numerical data, pointing out the complex interplay between QD and barrier recombination mechanisms. Nonetheless eq. 3 provides a simple expression to derive an indicative estimation of QD capture rate from the measured V_{oc} loss.

IV. Conclusion

The influence on the open circuit voltage of the reduction of the wetting layer and the inclusion of AlGaAs barriers during QD growth has been studied through a physics-based model accounting for QD dynamics and transport. QD morphology and their electronic states have been correlated through 8-band $k \cdot p$ simulations. Results show that wetting layer reduction is effective only in charged QDs, because the reduction of thermal coupling between barrier and QD states must occur along with a significant reduction of QD radiative recombination, which is only achievable by filling the QD confined states through doping. Nevertheless, wetting layer reduction is shown to reduce, at least to some extent, the doping density required for V_{oc} recovery. In this context it is worth noticing that the complete voltage recovery achieved in [13] is the result of substantial reduction of wetting layer confinement and low interdot modulation doping. The results presented here provide theoretical support to several experimental results in literature and suggest that doping and engineering of QD structure may hold further opportunities for high efficiency QDSCs.

V. Acknowledgement

Research was sponsored by the Army Research Laboratory and was accomplished under Cooperative Agreement Number W911NF-14-2-0040. The views and conclusions contained in this document are those of the authors and should not be interpreted as representing the official policies, either expressed or implied, of the Army Research Laboratory or the U.S. Government. The U.S. Government is authorized to reproduce and distribute reprints for Government purposes notwithstanding any copyright notation herein.

References

[1] Y. Okada, N. J. Ekins-Daukes, T. Kita, R. Tamaki, M. Yoshida, A. Pusch, O. Hess, C. C. Phillips, D. J. Farrell, K. Yoshida, N. Ahsan, Y. Shoji, T. Sogabe, and J.-F. Guillemoles, "Intermediate band solar cells: Recent progress and future directions," *Applied Physics Reviews*, vol. 2, no. 2, p. 021302, 2015.

[2] J. Wu, S. Chen, A. Seeds, and H. Liu, "Quantum dot optoelectronic devices: lasers, photodetectors and solar cells," *Journal of Physics D: Applied Physics*, vol. 48, no. 36, p. 363001, 2015.

[3] M. Gioannini, A. Cedola, N. Di Santo, F. Bertazzi, and F. Cappelluti, "Simulation of quantum dot solar cells including carrier intersubband dynamics and transport," *IEEE J. Photovolt.*, vol. 3, no. 4, pp. 1271–1278, Oct 2013.

[4] D. G. Sellers, S. Polly, S. M. Hubbard, and M. F. Doty, "Analyzing carrier escape mechanisms in inas/gaas quantum dot p-i-n junction photovoltaic cells," *Applied Physics Letters*, vol. 104, no. 22, 2014.

[5] T. Kita, R. Hasagawa, and T. Inoue, "Suppression of nonradiative recombination process in directly si-doped inas/gaas quantum dots," *Journal of Applied Physics*, vol. 110, no. 10, p. 103511, 2011.

[6] X. Yang, K. Wang, Y. Gu, H. Ni, X. Wang, T. Yang, and Z. Wang, "Improved efficiency of inas/gaas quantum dots solar cells by si-doping," *Solar Energy Materials and Solar Cells*, vol. 113, pp. 144–147, 2013.

[7] S. Polly, D. Forbes, K. Driscoll, S. Hellstrom, and S. Hubbard, "Delta-doping effects on quantum-dot solar cells," *IEEE J. Photovolt.*, vol. 4, no. 4, pp. 1079–10 857, 2014.

[8] P. Lam, S. Hatch, J. Wu, M. Tang, V. G. Dorogan, Y. I. Mazur, G. J. Salamo, I. Ramiro, A. Seeds, and H. Liu, "Voltage recovery in charged inas/gaas quantum dot solar cells," *Nano Energy*, vol. 6, pp. 159 – 166, 2014.

[9] F. Cappelluti, M. Gioannini, and A. Khalili, "Impact of doping on inas/gaas quantum-dot solar cells: a numerical study on photovoltaic and photoluminescence behavior," *Solar Energy Materials and Solar Cells*, vol. 157, pp. 209–220, 2016.

[10] F. K. Tutu, P. Lam, J. Wu, N. Miyashita, Y. Okada, K.-H. Lee, N. J. Ekins-Daukes, J. Wilson, and H. Liu, "Inas/gaas quantum dot solar cell with an alas cap layer," *Applied Physics Letters*, vol. 102, no. 16, p. 163907, 2013.

[11] K. Sablon, A. Sergeev, J. Little, N. Vagidov, and V. Mitin, "Nanoscale optimization of quantum dot media for effective photovoltaic conversion," in *SPIE Defense+ Security*. International Society for Optics and Photonics, 2014, pp. 908 313–908 313.

[12] D. Kim, M. Tang, J. Wu, S. Hatch, Y. Maidaniuk, V. Dorogan, Y. I. Mazur, G. J. Salamo, and H. Liu, "Si-doped inas/gaas quantum-dot solar cell with alas cap layers," *IEEE J. Photovolt.*, vol. PP, no. 99, pp. 1–6, 2016.

[13] A. Varghese, M. Yakimov, V. Tokranov, V. Mitin, K. Sablon, A. Sergeev, and S. Oktyabrsky, "Complete voltage recovery in quantum dot solar cells due to suppression of electron capture," *Nanoscale*, vol. 8, no. 13, pp. 7248–7256, 2016.

[14] "nextnano semiconductor software solutions," http://www.nextnano.com.

[15] S. Lee, O. L. Lazarenkova, P. von Allmen, F. Oyafuso, and G. Klimeck, "Effect of wetting layers on the strain and electronic structure of inas self-assembled quantum dots," *Physical Review B*, vol. 70, no. 12, p. 125307, 2004.

[16] A. Luque and A. Martí, "Increasing the efficiency of ideal solar cells by photon induced transitions at intermediate levels," *Phys. Rev. Lett.*, vol. 78, no. 26, pp. 5014–5017, 1997.

[17] A. Luque, A. Martí, and L. Cuadra, "Thermodynamic consistency of sub-bandgap absorbing solar cell proposals," *Electron Devices, IEEE Transactions on*, vol. 48, no. 9, pp. 2118–2124, 2001.

[18] K. A. Sablon, A. Sergeev, N. Vagidov, J. W. Little, and V. Mitin, "Effects of quantum dot charging on photoelectron processes and solar cell characteristics," *Solar Energy Mat. and Solar Cells*, 2012.

[19] F. Cappelluti, A. Musu, and A. Khalili, "Study of light-trapping enhanced quantum dot solar cells based on electrical and optical numerical simulations," in *2016 Compound Semiconductor Week (CSW) [Includes 28th International Conference on Indium Phosphide Related Materials (IPRM) 43rd International Symposium on Compound Semiconductors (ISCS)*, June 2016, pp. 1–2.

[20] A. Cuevas, "The recombination parameter {J0}," *Energy Procedia*, vol. 55, pp. 53 – 62, 2014, proceedings of the 4th International Conference on Crystalline Silicon Photovoltaics (SiliconPV 2014).

[21] V. Ryzhii, I. Khmyrova, V. Pipa, V. Mitin, and M. Willander, "Device model for quantum dot infrared photodetectors and their dark-current characteristics," *Semiconductor Science and Technology*, vol. 16, no. 5, p. 331, 2001.

[22] K. Sablon, A. Sergeev, N. Vagidov, A. Antipov, J. Little, and V. Mitin, "Effective harvesting, detection, and conversion of ir radiation due to quantum dots with built-in charge," *Nanoscale Research Letters*, vol. 6, no. 1, pp. 1–13, 2011.